

Cosmological constraints with the linear point from the BOSS survey

Mengfan He,^{1,2,3*} Cheng Zhao,^{4†} and Huanyuan Shan^{2,3‡}

¹National Astronomical Observatories, Chinese Academy of Sciences, Beijing 100012, China

²Shanghai Astronomical Observatory, Chinese Academy of Sciences, 80 Nandan Road, Shanghai 200030, China

³School of Astronomy and Space Science, University of Chinese Academy of Sciences, Beijing 100049, P.R. China

⁴Institute of Physics, Laboratory of Astrophysics, École Polytechnique Fédérale de Lausanne (EPFL), Observatoire de Sauverny, CH-1290 Versoix, Switzerland

Accepted XXX. Received YYY; in original form ZZZ

ABSTRACT

The *Linear Point* (LP), defined as the midpoint between the BAO peak and the associated left dip of the two-point correlation function (2PCF), $\xi(s)$, is proposed as a new standard ruler which is insensitive to nonlinear effects. In this paper, we use a Bayesian sampler to measure the LP and estimate the corresponding statistical uncertainty, and then perform cosmological parameter constraints with LP measurements. Using the Patchy mock catalogues, we find that the measured LPs are consistent with theoretical predictions at 0.6 per cent level. We find constraints with midpoints identified from the rescaled 2PCF ($s^2\xi$) more robust than those from the traditional LP based on ξ , as the BAO peak is not always prominent when scanning the cosmological parameter space, with the cost of 2–4 per cent increase of statistical uncertainty. This problem can also be solved by an additional dataset that provides strong parameter constraints. Measuring LP from the reconstructed data slightly increases the systematic error but significantly reduces the statistical error, resulting in more accurate measurements. The 1σ confidence interval of distance scale constraints from LP measurements are 20–30 per cent larger than those of the corresponding BAO measurements. For the reconstructed SDSS DR12 data, the constraints on H_0 and Ω_m in a flat- Λ CDM framework with the LP are generally consistent with those from BAO. When combined with Planck cosmic microwave background data, we obtain $H_0 = 68.02^{+0.36}_{-0.37}$ km s^{−1} Mpc^{−1} and $\Omega_m = 0.3055^{+0.0049}_{-0.0048}$ with the LP.

Key words: methods: data analysis – cosmological parameters – distance scale – large-scale structure of Universe

1 INTRODUCTION

The clustering of large-scale structures (LSSs) of the Universe allows measurements of the cosmic expansion history and structure growth through various physical effects such as baryon acoustic oscillations (BAO) and redshift space distortions (RSD). BAO is a result of primeval acoustic waves propagating in the coupled baryon-photon plasma before decoupling, observed as a peak in the two-point correlation function (2PCF) and as ripples in the power spectrum (PS). It provides us with a powerful standard ruler to map the expansion history of the Universe (Eisenstein et al. 1998, 2005; Bassett & Hlozek 2010). However, there are several physical effects that can shift or distort the peak in the CF, such as nonlinear gravitational evolution (Croce & Scoccimarro 2008), RSD and scale dependent bias (Smith et al. 2008).

The *Linear Point* (LP), defined as the midpoint between the BAO peak and the associated left dip of the 2PCF, $\xi(s)$, is insensitive to nonlinear gravity and can also be used as a standard ruler (Anselmi et al. 2016). The dependences of the LP and the BAO peak position on cosmological parameters are similar (O’Dwyer et al. 2020). It has been proved that the differences between the LP positions of linear

2PCF and Zel’dovich-approximated 2PCFs at different redshifts are consistent at 0.5 per cent level (Anselmi et al. 2016). In some previous analyses (Anselmi et al. 2016, 2018a,b), the LP position of a simulated 2PCF at low redshift is measured using a simple polynomial and then multiplied by 1.005 to restore agreement with linear prediction. Nikakhtar et al. (2021) proposed a Laguerre-based fitting and reconstruction method that provides more reliable LP measurements, especially when the correlation function does not show a clear peak or a dip around the BAO scale.

This purely geometric (PG) approach drops the reliance on the fiducial power spectrum, which is necessary for the standard template-based BAO analysis. It has been identified that LP is independent of the primordial cosmological parameters (Anselmi et al. 2016). Therefore, LP is promising for exploring cosmological models beyond Λ CDM. The forecast of s_{LP}/D_V (Anselmi et al. 2022), assuming DESI¹ (DESI Collaboration et al. 2016) and Euclid² (Laureijs et al. 2011), has a little larger uncertainty than standard template-based BAO measured r_d/D_V , but more accurate than results from *Purely-Geometric-BAO* (PG-BAO) method, which is a correlation-function model-fitting (CF-MF) analysis relies on a phenomenological cosmological model for the correlation function.

The comparison between the D_V derived from LP and BAO po-

* E-mail: mfhe@bao.ac.cn

† E-mail: cheng.zhao@epfl.ch

‡ E-mail: hyshan@shao.ac.cn

¹ <http://desi.lbl.gov>

² <http://sci.esa.int/euclid/>

sition measured from the Baryon Oscillation Spectroscopic Survey (BOSS; Dawson et al. 2013) LOWZ and CMASS data shows that the error of the D_V from LP analysis is less than that from the standard BAO method with the same pre-reconstruction data, but greater than that of BAO measurement from post-reconstruction data (Anselmi et al. 2018b). The BAO reconstruction, i.e., the process of eliminating nonlinear effects by reversing motions of galaxies (reference), has never been used in LP analysis because (1) the cosmology of reconstruction, which may deviate from the true cosmology, may bias the measurements (Anselmi et al. 2018b); (2) since LP is insensitive to nonlinear effects, reconstruction may not help much. However, given that the additional systematic error from BAO reconstruction is less than 0.1 per cent (Carter et al. 2020) and reconstruction is able to statistically improve the significance of the BAO peak, reconstruction still be relevant to the LP analysis and deserves careful investigation.

In this work, we improve the measurements and complete the analysis of LP based on the BOSS LRG dataset and the corresponding approximate mock catalogues. We use mocks to explore the performances of LP measurements with reconstruction and investigate the potential systematic biases and reliability of various LP measurement schemes. Since the statistical uncertainties are generally much larger than systematic biases for our samples, we use the quintic polynomial for measuring LP as in Anselmi et al. (2018a), rather than the more advanced method proposed by Nikakhtar et al. (2021) for simplicity. Furthermore, we perform cosmological parameter constraints for LP measurements from observational data for the first time.

The data and mock catalogues we used in this paper are introduced in Section 2. Then Section 3 presents the methodology for both the LP and BAO measurements. We explore the best LP measurement method and investigate the potential systematic bias using mock catalogues in Section 4, and apply our LP analysis to SDSS data and compare with the standard BAO analysis in Section 5. The results are concluded in Section 6.

2 DATA

From 2009 to 2014, the BOSS of SDSS–III Eisenstein et al. (2011) measured over 1.3 million LRG spectra using the double-armed spectrographs (Smee et al. 2013) as well as the 2.5-metre Sloan Telescope (Gunn et al. 2006) at the Apache Point Observatory. According to the different algorithms for target selection, the BOSS LRG dataset can be divided into LOWZ and CMASS populations, for galaxies with redshifts $z \lesssim 0.4$ and $0.4 < z < 0.7$, respectively. As the differences in clustering amplitude of subsamples with different target selection criteria are insignificant (Reid et al. 2016; Alam et al. 2017), the LOWZ and CMASS subsamples are combined as final SDSS Data Release 12 (DR12) LRG catalogue for LSS analysis. Moreover, BOSS DR12 also includes LRGs from SDSS–I/II (Abazajian et al. 2009). This dataset footprints in both northern and southern galactic caps (NGC and SGC) covering a total of nearly 10000 deg² sky. Following Alam et al. (2017), We divide the LRG catalogue into two non-overlapping redshift bins, $0.2 < z < 0.5$ and $0.5 < z < 0.75$, with the corresponding effective redshifts being 0.38 and 0.61 (e.g. Bautista et al. 2021, Section 2.5), respectively. We denote these two subsamples by ‘low- z ’ and ‘high- z ’ hereafter.

We use the DR12 MultiDark-Patchy (MD-Patchy) mock catalogues³ (Kitaura et al. 2016) to estimate covariance matrices for

2PCFs of DR12 LRG data, explore potential systematic bias and performance on cosmological parameter constraints for our LP analysis. The cosmological parameters of the MD-Patchy mocks are: $h = 0.6777$, $\Omega_m = 0.307115$, $\Omega_b h^2 = 0.02214$, $\sigma_8 = 0.8288$, $n_s = 0.9611$, $\Sigma m_V = 0$ eV, $r_d = 147.66$ Mpc.

The MD-Patchy mocks can reproduce the clustering of the BOSS DR12 data accurately since the PATCHY code takes advantages of structure formation model based on Augmented Lagrangian Perturbation Theory (ALPT; Kitaura & Hess 2013) and encodes nonlinear, stochastic, and non-local effects through galaxy biases (Kitaura et al. 2014). To investigate the effects of reconstruction on LP measurements, we examine for both pre- and post-reconstruction data. The reconstruction method used in BOSS DR12 galaxies and the corresponding MD-Patchy mocks following the algorithm introduced in Padmanabhan et al. (2012). The parameters used for reconstruction are $f=0.757$, $b=1.85$, $N_{\text{grid}} = 512^3$, the smoothing scale Σ_r is $15 h^{-1}$ Mpc. The NGC and SGC samples use the same parameters, but are processed separately since they are distributed far away from each other. In this work, the covariance matrices of pre-reconstruction data are estimated by 2048 independent realizations of DR12 MD-Patchy mocks, while the covariance matrices of post-reconstruction data are estimated by 1000 reconstructed MD-Patchy mocks.

3 METHODOLOGY

3.1 Correlation function estimator

Both the BAO peak and the LP position can be measured from the monopole two-point correlation functions (2PCFs). In this work, we use the Fast Correlation Function Calculator⁴ (FCFC; Zhao 2023) to calculate the pair counts of the data and random catalogues with the fiducial cosmology: $h = 0.6777$, $\Omega_m = 0.31$, $\Omega_b h^2 = 0.02214$, $\sigma_8 = 0.8288$, $n_s = 0.9611$, $\Sigma m_V = 0.06$ eV. Then the 2PCFs are estimated through combined pair counts using the Landy–Szalay (LS) estimator (Landy & Szalay 1993):

$$\xi = \frac{DD - 2DR + RR}{RR}. \quad (1)$$

Here, the D and R indicate the data and random catalogues, respectively. For the reconstructed galaxy sample, the 2PCF estimator is slightly different, as:

$$\xi = \frac{DD - 2DS + SS}{RR}, \quad (2)$$

in which S stands for the shifted random catalogue, which is generated by moving random objects with the same displacement field for galaxy reconstruction.

Since each mock consists of two datasets corresponding to NGC and SGC, we combine these two datasets following Zhao et al. (2022) at the pair count level. In this work, the 2PCFs we used are all calculated with the combination of NGC and SGC.

3.2 LP measurements

3.2.1 LP detection

The fiducial cosmology used to convert the measured angles and redshifts into comoving coordinates may deviate from the true cosmology, leading to the Alcock–Paczynski (AP) distortion effect. The

³ https://data.sdss.org/sas/dr12/boos/lss/dr12_multidark_patchy_mocks/

⁴ <https://github.com/cheng-zhao/FCFC>

effect in the 2PCF monopole can be mitigated by rescaling the distance s by the isotropic-volume-distance D_V (Sánchez et al. 2012). The relation between the true and fiducial CF is:

$$\xi_0(s^{\text{fid}}/D_V^{\text{fid}}) \simeq \xi_0(s^{\text{true}}/D_V^{\text{true}}), \quad (3)$$

where

$$D_V(z) = \left[(1+z)^2 D_A^2(z) \frac{cz}{H(z)} \right]^{1/3}, \quad (4)$$

in which D_A is the angular diameter distance, $H(z)$ is the Hubble rate, and c is the speed of light. Following Anselmi et al. (2018a), the CF can be fitted with a 5th-order polynomial,

$$\xi_{\text{fit}}(s) = \sum_{i=0}^5 a_i s^i, \quad (5)$$

with an s bin of $3 h^{-1} \text{Mpc}$ and fitting range of $60\text{--}130 h^{-1} \text{Mpc}$. The polynomial fits are performed using the Markov Chain Monte Carlo (MCMC) method with `emcee`⁵ (Foreman-Mackey et al. 2013). We consider 32 walkers with 15000 sampling steps each, then remove the first 10000 steps of each walker as burn-in period.

Then the LP position can be calculated by

$$s_{\text{LP}} = \frac{1}{2}(s_{\text{peak}} + s_{\text{dip}}), \quad (6)$$

where s_{peak} and s_{dip} are, respectively, the BAO peak and its associated left dip, which can be obtained by searching for points within the range of $s \in [70, 115] h^{-1} \text{Mpc}$ that satisfy $d\xi_{\text{fit}}/ds = 0$. The final measurement of LP is given by

$$y_{\text{LP}} = s_{\text{LP}}/D_V. \quad (7)$$

However, s_{LP} defined by Eq. (6) is not always measurable from the Patchy mocks in practice, as the BAO feature of the 2PCF is not always prominent due to cosmic variances, especially for the pre-reconstruction case. If this happens often, the LP position measurements would be unreliable. Therefore, we also measure the LP positions from rescaled 2PCFs of $s^2\xi$, which amplifies the significance of the BAO peak, that is, the BAO peak and its associated left dip are calculated by $d(s^2\xi_{\text{fit}})/ds = 0$. Moreover, BAO reconstruction is foreseen to help settling the problem, as it is expected to statistically improve the significance of the BAO peak. The comparisons between the two LP detection schemes and the measurements based on pre- and post-reconstruction data are detailed in Section 4.

3.2.2 Error estimation

In Anselmi et al. (2018a), the uncertainty on the LP position is normally estimated by propagating the uncertainties of the fitted polynomial coefficients (error propagation, EP hereafter). The formula can be written as follows:

$$\sigma_{s_{\text{LP}}} = A \cdot C \cdot A^T, \quad (8)$$

in which C is the covariance matrix of the polynomial coefficients from the MCMC sampler, and

$$A = \left[\frac{\partial s_{\text{LP}}}{\partial a_1}, \frac{\partial s_{\text{LP}}}{\partial a_2}, \dots, \frac{\partial s_{\text{LP}}}{\partial a_n} \right], \quad (9)$$

with

$$\frac{\partial s_{\text{LP}}}{\partial a_i} = \frac{s_{\text{LP}}(a_i + \epsilon_i) - s_{\text{LP}}(a_i - \epsilon_i)}{2 * \epsilon_i}, \quad (10)$$

where a_i indicate the best-fitting polynomial coefficients. We test ϵ_i in the range $10^{-10} a_i < \epsilon_i < 10^{-4} a_i$, and find that $\sigma_{s_{\text{LP}}}$ is stable with $10^{-9} a_i < \epsilon_i < 10^{-6} a_i$.

In this paper, we also consider another scheme for fitted error estimation, the Bayesian samplers, which is expected to be more promising. For fitted polynomial coefficients in Monte-Carlo Bayesian posterior sampling, the posterior distribution of y_{LP} is obtained by calculating y_{LP} as a derived parameter from fitted coefficients. And then the 1σ statistical uncertainty can be estimated by mean of 16th and 84th percentage of the posterior distribution of y_{LP} . The comparison between Bayesian samplers (MCMC hereafter) and error propagation methods will be described in Section 4.

3.3 BAO measurements

The position of the BAO peak can be measured by traditional template fitting (Xu et al. 2012), which can be defined as:

$$\xi_{\text{model}}(s) = B^2 \xi_t(\alpha s) + A(s), \quad (11)$$

where B is normalization factor, $A(s)$ term consists of nuisance parameters accounting for the broad band signal in correlation function with:

$$A(s) = a_0 s^{-2} + a_1 s^{-1} + a_2, \quad (12)$$

and ξ_t indicates the template correlation function:

$$\xi_t(s) = \int \frac{k^2 dk}{2\pi^2} P_t(k) j_0(ks) e^{-k^2 a^2}, \quad (13)$$

which is a Hankel transform of a template power spectrum P_t , and j_0 is the 0-order spherical Bessel function $j_0 = \sin(kr)/kr$, $a = 1 h^{-1} \text{Mpc}$ is a parameter to reduce numerical instability of the integration. The template power spectrum P_t is defined by:

$$P_t(k) = [P_{\text{lin}} - P_{\text{smooth}}] e^{-k^2 \Sigma_{\text{NL}}^2/2} + P_{\text{smooth}}(k), \quad (14)$$

where P_{lin} is the linear power spectrum, and P_{smooth} is the no-wiggle power spectrum, Σ_{NL} is a BAO damping parameter that is used to model the degradation in the acoustic peak due to nonlinear evolution.

There are 6 parameters (B^2 , α , Σ_{NL} , a_1 , a_2 , a_3) in BAO model. The critical parameter α quantifies the dilation of the measured correlation function relative to the template correlation function, it is essentially a measurement of the BAO peak. Our BAO fitting range is $30\text{--}180 h^{-1} \text{Mpc}$ with the bin size of $3 h^{-1} \text{Mpc}$. We set flat priors for the parameters (α , B , Σ_{NL}) in the ranges of $([0.8, 1.2], [0, 10], [0, 20]) h^{-1} \text{Mpc}$, respectively. The priors of the parameters are large enough compared to the posterior distributions.

With the fitted α , we can obtain $D_V(z)/r_d$ based on the fiducial value of the template by

$$D_V(z)/r_d = \alpha \times D_{V,\text{fid}}/r_{d,\text{fid}}, \quad (15)$$

which is used to perform cosmological parameter constraints.

3.4 Cosmological parameter constraints

We use the `COBAYA`⁶ package to constrain cosmological parameters with LP and BAO measurements. `COBAYA` is a MCMC sampler implemented in `PYTHON`. In this work, we consider the standard flat- Λ CDM

⁵ <https://github.com/dfm/emcee>

⁶ <https://github.com/CobayaSampler/cobaya>

cosmology, with alternative probes including the Big Bang Nucleosynthesis (BBN) calculations with primordial deuterium abundance (Cooke et al. 2018), which provides the constraints on r_d , as well as the Planck CMB temperature and polarization data (Planck Collaboration et al. 2020), to break parameter degeneracies and achieve better cosmological constraints. For both constraints with LP and BAO, the convergence stop criteria are set into the potential scale reduction factor, $R - 1 = 0.01$. For each chain, we remove the first 30 per cent samples as burn in period.

The likelihood of cosmological parameters \mathbf{p} is:

$$\mathcal{L} \approx e^{-\chi^2(\mathbf{p})/2}. \quad (16)$$

Since datasets that we used in this paper are independent, here chi-squared function χ^2 can be calculated by

$$\chi^2(\mathbf{p}) = \sum_{z \text{ bins}} (y_{\text{LP,data}} - y_{\text{LP,model}}(\mathbf{p}))^2 / \sigma_y^2, \quad (17)$$

where $y_{\text{LP,data}}$ is best-fitting y_{LP} measured from data, and $y_{\text{LP,model}}$ is y_{LP} measured from theoretical 2PCFs generated using CAMB⁷ software with sampled cosmological parameters. The measuring schemes for $y_{\text{LP,data}}$ and $y_{\text{LP,model}}$ are the same, for example, if $y_{\text{LP,data}}$ is measured from a rescaled 2PCF, $y_{\text{LP,model}}$ is also measured from a rescaled 2PCF, but for a theoretical one. Note that for theoretical 2PCFs in different cosmology, the searching range of BAO peak and its associated left dip is $s \in [0.7r_d, 1.2r_d]$. r_d denotes the comoving sound horizon at the drag epoch in the corresponding cosmology. The formulae for the BAO measurements are the same as those for the LP measurements, but with y_{LP} replaced by D_v/r_d .

4 RELIABILITY AND ERROR ANALYSIS USING MOCK CATALOGUES

We have introduced some LP measurement schemes which may lead to different best-fitting values and errors of the LP. In this section, we will take advantage of Patchy mocks to compare these measurement schemes from three aspects: reliability, systematic bias and statistical error, to figure out the optimal scheme for LP analysis.

4.1 Reliability

As we mentioned before, if the BAO feature of the 2PCF is not prominent, s_{LP} would not be measurable. The reliability of LP measurement can be characterized using the proportion of the s_{LP} -measurable 2PCFs in all mock realizations.

We show the s_{LP} -measurable 2PCF fraction of the best-fitting 2PCFs of the mock realizations, as well as the averaged $N_{\text{peak,MC}}/N_{\text{all,MC}}$ over all realizations in Table 1, where $N_{\text{all,MC}}$ refers to the total number of MCMC iterations, and $N_{\text{peak,MC}}$ indicates the number of iterations with s_{LP} measurable.

For the pre-reconstruction case, 23–40 per cent of plain 2PCFs are not s_{LP} -measurable, indicating that LP measurements from the pre-reconstruction case are unreliable. We then tested the reconstruction and 2PCF rescaling that amplify the significance of the BAO peak. With BAO reconstruction, the s_{LP} -measurable rate becomes over ~95 per cent, and the rescaling increased the s_{LP} -measurable rate to over ~90 per cent. When both operations are used, the s_{LP} -measurable rate can be higher than 98 per cent.

Sample	ξ		$s^2\xi$	
	MCMC	best	MCMC	best
pre-recon (low-z)	60.6%	66.8%	91.5%	98.4%
pre-recon (high-z)	66.8%	77.3%	96.1%	99.5%
post-recon (low-z)	94.9%	99.6%	98.9%	100.0%
post-recon (high-z)	96.1%	99.5%	99.4%	99.9%

Table 1. The percentage of s_{LP} -measurable 2PCFs of individual mocks. Columns (second and third) labeled with ξ shows measurements from plain 2PCFs, while $s^2\xi$ refers to rescaled 2PCFs. The values in ‘MCMC’ column denoted the mean of $N_{\text{peak,MC}}/N_{\text{all,MC}}$ of mocks, $N_{\text{all,MC}}$ refers to total number of MCMC iterations, and $N_{\text{peak,MC}}$ indicates the number of iterations with s_{LP} measurable. The ‘best’ columns show s_{LP} -measurable mock fractions.

4.2 Systematic bias

The systematic biases of y_{LP} are estimated by the difference between the fitted values of mean 2PCFs of mocks and the theoretical prediction. To eliminate the potential influence of statistical uncertainty, the covariance measured using the mocks is rescaled by $1/N_{\text{mocks}}$, where N_{mocks} indicates the total number of mocks.

We show the systematic biases expressed in terms of a percentage in Table 2. The columns under ‘ Δy_{lin} ’ show $\Delta y/y_{\text{LP,lin}}$ with $\Delta y = y_{\text{LP,fit}} - y_{\text{LP,lin}}$, in which $y_{\text{LP,lin}}$ is y_{LP} predicted by linear theory, and $y_{\text{LP,fit}}$ is the best-fitting y_{LP} of mean 2PCFs of mocks. Best-fitting y_{LP} can be estimated either as the median value of posterior distribution of y_{LP} or as the value corresponding to the minimum χ^2 , denoted as ‘best-fitting (median)’ and ‘best-fitting (min)’, respectively. For the measurements from the rescaled 2PCFs, both the best-fitting and the theoretical predicted y_{LP} are measured from the rescaled 2PCFs. It shows that systematic biases are all greater than 1.04 per cent.

Since nonlinear effects can smooth and shift the BAO peak in CF, resulting in differences between the LP position predicted by linear theory and the measured one. We check also the Zel’dovich-approximated theoretical 2PCFs with the results from mean 2PCFs of mocks. The Zel’dovich-approximated 2PCFs can be calculated as

$$\xi^{\text{zel}}(s) = \int \frac{dk}{k} \frac{k^3 P_{\text{lin}}(k)}{2\pi^2} e^{-k^2 \sigma_v^2(z)} j_0(ks), \quad (18)$$

where

$$\sigma_v^2 = \frac{1}{3} \int \frac{d^3q}{(2\pi)^3} \frac{P_{\text{lin}}(q, z)}{q^2} \quad (19)$$

is the square of linear displacement field dispersion and the damping scale $k_{NL} = 1/\sigma_v$.

Then Zel’dovich-approximated $y_{\text{LP,zel}}$ can be estimated from ξ^{zel} . We show the biases estimated by $(y_{\text{LP,fit}} - y_{\text{LP,zel}})/y_{\text{LP,zel}}$ in Table 2. We find that $y_{\text{LP,fit}}$ are significantly more consistent with $y_{\text{LP,zel}}$ than $y_{\text{LP,lin}}$, and the biases are less than 0.6 per cent for all cases. BAO reconstruction slightly increases the systematic bias. In this case, the median value of y_{LP} posterior distribution is closer to the theoretically predicted $y_{\text{LP,zel}}$ than the corresponding minimum- χ^2 value.

The measurements from the rescaled post-reconstruction 2PCFs show the largest Δy_{zel} , and the lowest Δy_{lin} , which may be due to the mitigation of nonlinear effects by reconstruction. However, given the fact that $y_{\text{LP,zel}}$ is more consistent with y_{LP} measured from mean 2PCFs of mocks, the Zel’dovich approximation 2PCFs are adopted as theoretical 2PCFs of $y_{\text{LP,model}}$ (Eq. 17) for cosmological parameter constraints, and Δy_{zel} will be included in the error estimation.

We also explore the potential systematic error with the fiducial cosmological parameter $\Omega_m = \{0.12, 0.25, 0.31, 0.64, 0.85\}$, show-

⁷ <https://camb.info/>

Sample	ξ				$s^2\xi$			
	Δy_{lin}		Δy_{zel}		Δy_{lin}		Δy_{zel}	
	med	min	med	min	med	min	med	min
pre-recon (low-z)	1.35%	1.43%	0.28%	0.21%	1.59%	1.66%	0.04%	0.03%
pre-recon (high-z)	1.38%	1.32%	0.26%	0.31%	1.57%	1.48%	0.06%	0.15%
post-recon (low-z)	1.43%	1.30%	0.21%	0.33%	1.17%	1.04%	0.47%	0.60%
post-recon (high-z)	1.43%	1.38%	0.20%	0.25%	1.22%	1.16%	0.42%	0.48%

Table 2. The potential systematic bias estimated by mean 2PCF of Patchy mocks. The columns under ‘ Δy_{lin} ’ show $(y_{\text{LP,fit}} - y_{\text{LP,lin}})/y_{\text{LP,lin}}$ with $y_{\text{LP,lin}}$ being y_{LP} predicted by linear theory, and $y_{\text{LP,fit}}$ is the best-fitting y_{LP} of mean 2PCFs of mocks, which can be estimated by the median value of the posterior distribution of y_{LP} (shown in ‘med’ column) and y_{LP} value corresponding to minimum reduced χ^2 (shown in ‘min’ column). Δy_{zel} is similar to Δy_{lin} , but replacing $y_{\text{LP,lin}}$ with $y_{\text{LP,zel}}$ estimated from the Zel’dovich-approximated 2PCFs.

ing that the measured LPs are still consistent with the theoretically predicted values ($y_{\text{LP,zel}}$) at 0.6 per cent level (see Appendix A).

Note that the systematic error of y_{LP} can be further reduced by measuring LP using the Laguerre reconstruction method (Nikakhtar et al. 2021); we leave the relevant studies for future work.

4.3 Statistical uncertainty

The statistical uncertainty is crucial for cosmological constraints with LP, therefore it is important to identify the LP measurement scheme that provides the most reliable statistical uncertainty. In this subsection, we compare the statistical errors of s_{LP} measured with different schemes. We show the 1σ statistical errors of s_{LP} ($\sigma_{s_{\text{LP}}}$) estimated from the mean 2PCFs of the mocks and the 2PCFs of the individual mocks in Table 3.

To set a solid reference for the comparison, we rescale the covariance matrix by $1/N_{\text{mocks}}$ when fitting to the mean 2PCFs of mocks, thus the cosmic variance is highly reduced. Then, we rescale the fitted error of the LP by $\sqrt{N_{\text{mocks}}}$, so the value is directly comparable to that from individual mocks.

Comparing to the 1σ dispersion of best-fitting (min) s_{LP} distribution of all mocks (σ_{min}), the measurements from best-fitting (median) s_{LP} , i.e., σ_{med} are more consistent with σ_{CR} , suggesting that the median value is a better indicator of the best-fitting value.

The statistical errors measured by MCMC method, including measurements from mean 2PCFs of mocks (σ_{MC}) and median value of $\sigma_{s_{\text{LP}}}$ from individual mocks ($\tilde{\sigma}_{\text{MC}}$), are consistent with each other, and generally more consistent with σ_{med} than corresponding measurements from the EP method. Moreover, the EP method also shows higher systematic error. Thus, MCMC is a more reliable method for statistical uncertainty estimation.

We show the fitted posterior distributions of y_{LP} from the mean 2PCFs of the mocks (orange lines) and the distribution of best-fitting (median) y_{LP} of individual mocks (blue histograms) in Figure 1. The posterior of y_{LP} fitted from mean 2PCFs of mocks show good agreement with the distributions of mock realizations for both measurements from plain (upper two rows) and rescaled 2PCFs (bottom two rows), suggesting that the posteriors of y_{LP} are unbiased and the values derived from the posteriors are reliable.

The comparison of statistical errors from the plain and rescaled 2PCFs shows that measuring the LP position from the rescaled 2PCFs increases the statistical error by 2–9 per cent without reconstruction and by 2–4 per cent for the post-reconstruction case. Note however that the measurements from pre-reconstruction plain 2PCFs may not be reliable due to the low s_{LP} -measurable rate. Comparing the results on the rescaled 2PCFs with and without BAO reconstruction, we can find that reconstruction significantly reduces the statistical uncertainty by 20–30 per cent.

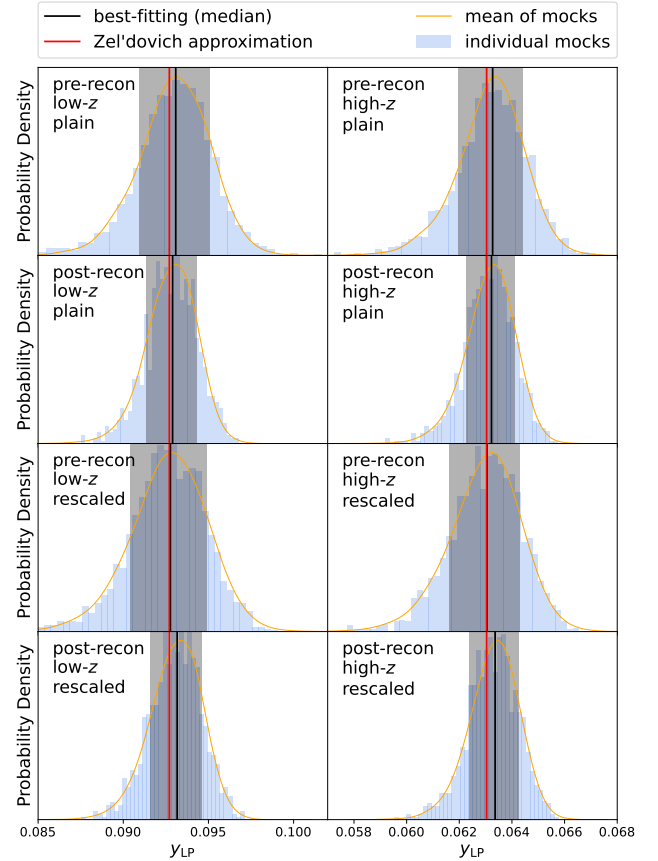


Figure 1. The fitted posterior distributions of y_{LP} for the mean 2PCFs of all mocks (orange lines) and distributions of best-fitting (median) y_{LP} of individual mocks (blue histograms). The black vertical line and grey shadows indicate the 50th and range of 16th to 84th percentiles of the cumulative posterior distribution of y_{LP} for the mean 2PCFs of all mocks, respectively. The red vertical lines show the expected y_{LP} from theoretical Zel’dovich-approximated 2PCFs. The upper two rows show two redshift bins of pre-reconstruction, while the bottom two rows show the results of post-reconstruction

In summary, statistical errors estimated by EP method are less stable than MCMC method and best-fitting (median) outperforms best-fitting (min). Therefore, we use best-fitting value given by median value of posterior distribution of y_{LP} , and the statistical error measured by the MCMC method for the following LP measurements.

Sample	ξ							$s^2\xi$						
	mean of mocks			individual mocks				mean of mocks			individual mocks			
	σ_{CR}	σ_{MC}	σ_{EP}	σ_{med}	σ_{min}	$\tilde{\sigma}_{\text{MC}}$	$\tilde{\sigma}_{\text{EP}}$	σ_{CR}	σ_{MC}	σ_{EP}	σ_{med}	σ_{min}	$\tilde{\sigma}_{\text{MC}}$	$\tilde{\sigma}_{\text{EP}}$
pre (low-z)	2.21	2.05	2.36	2.07	1.85	1.99	1.78	2.27	2.24	2.03	2.18	2.10	2.17	2.06
pre (high-z)	1.91	1.81	1.56	1.89	1.69	1.78	1.64	1.95	1.96	2.99	1.96	1.83	1.92	1.81
post (low-z)	1.46	1.47	1.43	1.47	1.32	1.48	1.40	1.52	1.52	1.62	1.50	1.40	1.53	1.51
post (high-z)	1.33	1.36	1.12	1.32	1.26	1.36	1.30	1.37	1.38	1.21	1.34	1.29	1.38	1.33

Table 3. The statistical errors of s_{LP} . The columns label with ‘mean of mocks’ show the mean of the lower and upper 1σ confidence limits of s_{LP} fitted from the mean 2PCFs of mocks. Among them, σ_{CR} indicates errors measured from fittings with the covariances rescaled by $1/N_{\text{mocks}}$ and then the 1σ confidence intervals multiplied by $\sqrt{N_{\text{mocks}}}$. The σ_{MC} and σ_{EP} indicate errors measured with MCMC and error propagation method respectively. Notes that except the ‘ σ_{CR} ’ column, all of the statistical error show in this table are measured with the covariances are not rescaled. Columns labeled with ‘individual mocks’ show measurements from individual mocks, σ_{med} and σ_{min} are the 1σ dispersion of best-fitting (median) and best-fitting (min) s_{LP} distribution of all mocks, respectively. $\tilde{\sigma}_{\text{MC}}$ and $\tilde{\sigma}_{\text{EP}}$ are the median values of the fitted errors $\sigma_{s_{\text{LP}}}$ of individual mocks estimated by the MCMC method and the EP method, respectively.

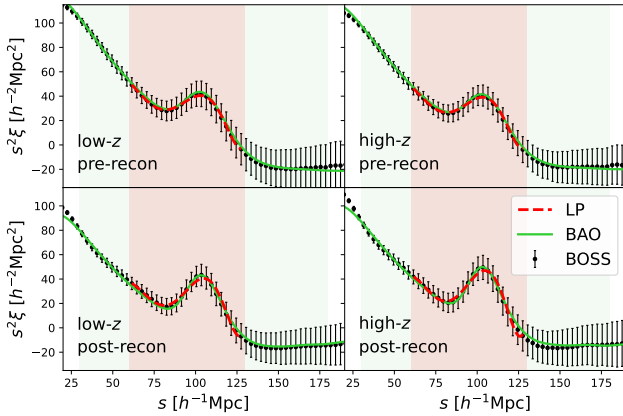


Figure 2. The mean 2PCFs of all Patchy mocks of different samples. The dots show the mean 2PCFs of all Patchy mocks, with error bars being the standard deviation of measurements from realizations of the corresponding Patchy mocks. The dashed red lines show the best-fitting 5th-order polynomial models. The best-fitting 2PCFs from BAO template fitting are shown with solid green lines. The orange shadow areas are the fitting ranges of polynomial fitting (60–130 $h^{-1}\text{Mpc}$) and the green ranges are that of BAO fitting (30–180 $h^{-1}\text{Mpc}$). The upper panels show pre-reconstruction measurements, while bottom panels show post-reconstruction’s.

4.4 LP and BAO fitting results

We compare the LP and BAO measurements from mean 2PCFs of Patchy mocks. The resulting 2PCFs are shown in Figure 2 with the corresponding posterior distributions of the parameters y_{LP} and α illustrated in Figure 3. The fitted 2PCFs generally agree well with the mean 2PCFs of mocks in their fitting range, but the fitted 2PCFs described by the 5th-order polynomial show larger deviations than the 2PCFs fitted with BAO template fitting, especially at the large end of the fitting range. Figure 3 shows that the distributions of the post-reconstruction data (orange and yellow) are more concentrated than those without reconstruction, especially for the redshift bin $z \in [0.2, 0.5]$, and the distributions of y_{LP} measured from plain 2PCFs are slightly more concentrated than the measurement from rescaled 2PCFs, which is consistent with our findings in the last subsection.

We also plot the distribution of best-fitting values of y_{LP} and α in Figure 4. The black dashed lines indicate the theoretical predicted y_{LP} as a function of α , which is calculated by:

$$y = \frac{1}{(D_{\text{V}}/s_{\text{LP}})_{\text{true}} \times \alpha}, \quad (20)$$

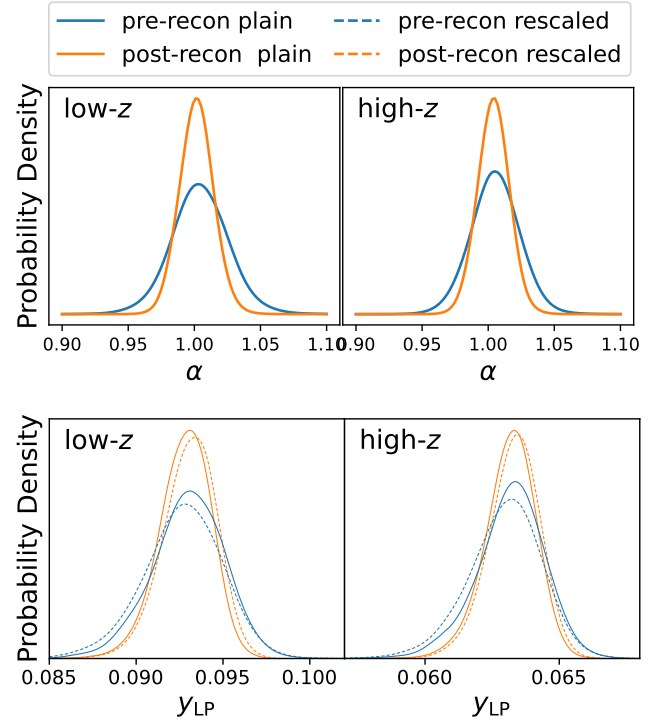


Figure 3. The marginalized posterior distribution of α and y_{LP} fitted from the mean 2PCFs of the mocks. The blue lines show measurements from pre-reconstruction data, while measurements from post-reconstruction data are shown with orange lines. The distribution of y_{LP} measured from SDSS data are illustrated in bottom two panels, the dashed lines show distributions of y_{LP} that measured from rescaled 2PCFs, while the solid lines indicate distributions of y_{LP} that measured from plain 2PCFs.

where $(D_{\text{V}}/s_{\text{LP}})_{\text{true}}$ is calculated by CAMB with the cosmology of Patchy mocks, the grey shadow areas denote 1σ statistical error of y_{LP} and α . The systematic error of y_{LP} is computed using $y_{\text{LP,zel}}$, as discussed in Section 4, and the systematic error of α is defined as:

$$\Delta\alpha = \alpha_{\text{best}} - \alpha_{\text{exp}}, \quad (21)$$

where α_{exp} is estimated by

$$\alpha_{\text{exp}} = \frac{D_{\text{V}}^{\text{true}}/r_{\text{d}}^{\text{true}}}{D_{\text{V}}^{\text{fid}}/r_{\text{d}}^{\text{fid}}}, \quad (22)$$

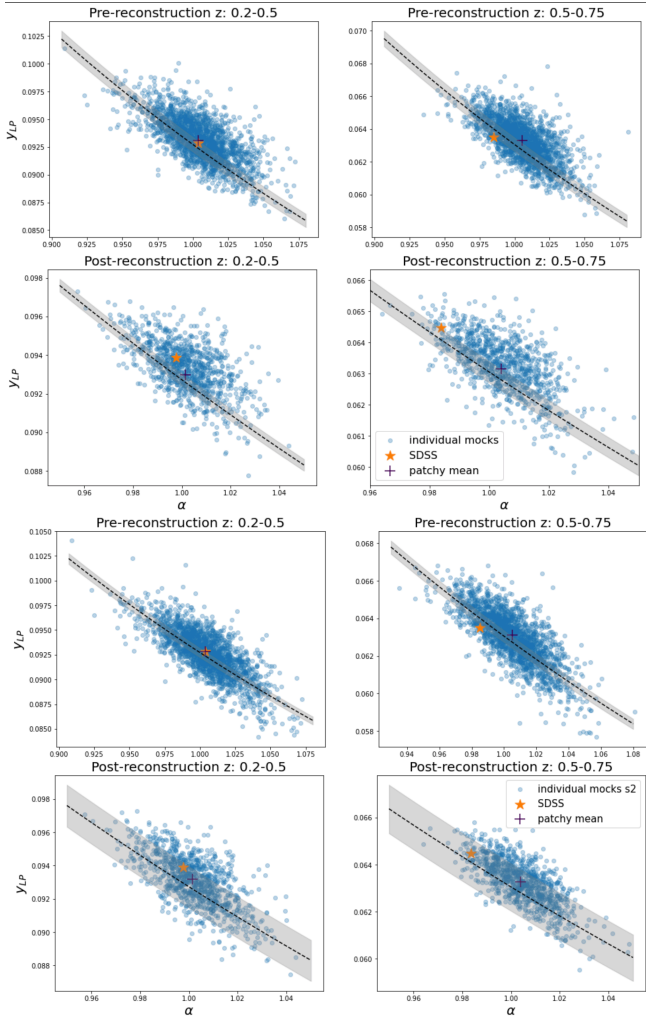


Figure 4. Distribution of the best-fitting value of y_{LP} and α . The upper two rows show the y_{LP} estimated from plain 2PCFs while the rest two rows show measurements from rescaled 2PCFs. The blue scatter points illustrate the measurements from individual mocks. Purple plus symbols shows best-fitting values from the mean 2PCFs of Patchy mocks, while the yellow star symbols indicate the best-fitting values from SDSS data. The black dashed lines and grey shadow areas show the theoretical predicted values defined as Eq. 20 and the corresponding systematic bias range.

and α_{best} denotes the best-fitting α of mean 2PCF of mocks with the covariance matrix rescaled by $1/N_{\text{mocks}}$.

Figure 4 shows that α and y_{LP} are highly anti-correlated. The values from individual mocks are distributed around the theoretical predicted line, so do the measurements from data and mean of all Patchy mocks. It is consistent with the theoretical predictions after taking into account the systematic errors discussed in Section 4.

The measurements of y_{LP} and α are summarised in Table 4, in which $\sigma_{\text{comb}} = \sqrt{\Delta^2 + \sigma^2}$ indicates the combined error of systematic bias Δ and statistical error σ , which is used for cosmological analysis. The combined error of y_{LP} is dominated by the statistical error, since the potential systematic bias (difference between the black and red vertical lines in Figure 1) is much less than the statistical error (shadow range in Figure 1). For y_{LP} measurement, BAO reconstruction is able to reduce the combined error by 25–32 per cent. Though with the rescaled 2PCF the LP measurements are more reliable, the statistical errors become 5–8 per cent larger. Comparing the

post-reconstruction results with the corresponding α measurements, the 1σ confidence interval of y_{LP} is 20–30 per cent larger.

4.5 Cosmological parameter measurements

We convert the best-fitting α to $D_{\text{v}}/r_{\text{d}}$ measurements, and then perform cosmological parameter constraints in the standard flat- Λ CDM cosmological model with different $D_{\text{v}}/r_{\text{d}}$ measurements and y_{LP} measurements from mean 2PCFs of mocks.

The constraints of H_0 and Ω_{m} from the combination of the BBN and y_{LP} measurements (BBN + LP) and the combination of the BBN and $D_{\text{v}}/r_{\text{d}}$ measurements (BBN + BAO) are shown in Figure 5 and Table 5. Note that all measurements are from reconstructed data. Compared to the constraints from the BBN + LP (rescaled), i.e., right panel of Figure 5, the constraints of the plain 2PCFs (left panel of Figure 5) are tighter and concentrated at lower value. However, this does not necessarily mean that the measurement of LP from plain 2PCFs is better than the rescaled 2PCFs.

In fact, Figure 6, which shows the 2PCFs at cosmology shown with red star in left panel of Figure 5, suggests that for both the linear and Zel’dovich 2PCFs, when Ω_{m} and H_0 are larger, the BAO peak and dips are not clear or ill-behaved in the plain 2PCFs and thus non-detectable, while for the rescaled 2PCFs they are easily identified by our LP finding algorithm. Therefore, the exclusion of large Ω_{m} and H_0 values by the LP measurements may be due to the weakness of the LP identification method with the plain 2PCFs.

It means that the LP constraints with the rescaled 2PCFs are more reliable. The constraints of BBN + LP (rescaled) and BBN + BAO are similar, which is consistent with the highly correlated LP and BAO measurements shown in Figure 4. However, compared to the BBN + BAO results, the constraints from BBN + LP have a 21 per cent larger 1σ confidence interval and a 0.57σ larger bias of the best-fitting value in Ω_{m} , as well as a 3.6 per cent larger 1σ confidence interval and a 0.62σ larger bias of the best-fitting value in H_0 .

Even with the rescaled 2PCFs, the LP may still be undetectable for extreme Ω_{m} and H_0 values. This problem can be solved by including additional observational datasets, so that the Ω_{m} and H_0 values are better constrained. For this reason, we explore cosmological constraints with the combination of the LP measurement and Planck CMB data (Planck Collaboration et al. 2020). The CMB + LP and CMB + BAO results are shown in Figure 7. It shows that the constraints of CMB + LP and CMB + BAO are highly consistent, even though the errors of CMB + LP are slightly larger than those of CMB + BAO. The results from the plain and rescaled 2PCFs are almost identical. Since the systematic error of LP measured from the plain 2PCF is smaller than that of the rescaled one (Section 4.2), we focus on the CMB + LP (plain) results for cosmological analysis hereafter.

5 RESULTS

In this section, we present our LP measurements using the SDSS data and provide the corresponding cosmological constraints. Furthermore, we compare our results with the measurements from the template-based BAO fitting method.

5.1 Fitting results

We perform polynomial fits for 2PCFs from the SDSS data as the fitting scheme we applied in mocks. The best-fitting 2PCFs are shown in Figure 8, along with the 2PCFs measured from the SDSS data. Both the polynomial model and the template model agree well with

Patchy mock	measurement	best-fitting	Δ	σ	σ_{comb}	$\sigma_{\text{comb}}(\%)$	$\frac{\chi^2}{\text{d.o.f}}$
pre (low-z)	$100 \times y_{\text{LP}}(\xi)$	9.308	0.026	0.206	0.208	2.2%	3.55
	$100 \times y_{\text{LP}}(s^2\xi)$	9.276	0.004	0.225	0.225	2.4%	
	α	1.0038	0.0045	0.021	0.021	2.1%	
pre (high-z)	$100 \times y_{\text{LP}}(\xi)$	6.327	0.016	0.123	0.124	2.0%	3.51
	$100 \times y_{\text{LP}}(s^2\xi)$	6.306	0.004	0.134	0.134	2.1%	
	α	1.0052	0.0042	0.018	0.019	1.9%	
post (low-z)	$\text{LP}(\xi)$	9.289	0.019	0.147	0.148	1.6%	9.20
	$100 \times y_{\text{LP}}(s^2\xi)$	9.316	0.044	0.153	0.159	1.7%	
	α	1.0016	0.0015	0.013	0.013	1.3%	
post (high-z)	$100 \times y_{\text{LP}}(\xi)$	6.322	0.013	0.093	0.094	1.5%	8.00
	$100 \times y_{\text{LP}}(s^2\xi)$	6.336	0.026	0.094	0.098	1.5%	
	α	1.0040	0.0036	0.012	0.012	1.2%	

Table 4. The measured y_{LP} and α from the mean 2PCFs of the mocks. Note that all values of the y_{LP} measurements, except ' $\sigma_{\text{comb}}(\%)$ ', are multiplied by 100. Δ column shows systematic biases measured from the fittings to the mean of patchy mock with covariances rescaled by $1/N_{\text{mock}}$. σ and σ_{comb} columns show the statistical errors and combined error $\sigma_{\text{comb}} = \sqrt{\Delta^2 + \sigma^2}$, respectively. $\frac{\chi^2}{\text{d.o.f}}$ shows the best-fit reduced χ^2 of corresponding models, note that χ^2 are estimated with normalized covariance matrices and d.o.f indicates degree of freedom.

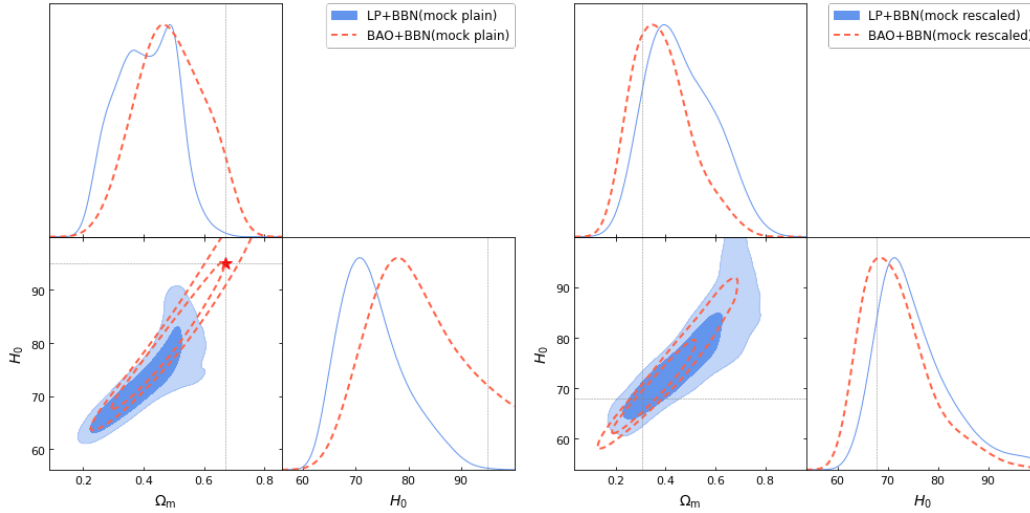


Figure 5. Constraints on H_0 and Ω_m based on combination of BBN and measurements from reconstructed mocks. The blue contour and lines show constraints from BBN + LP, while the red dashed contour and lines show that of BBN + BAO. The left panel shows result of LP measured from plain 2PCFs and the right panel is for LP from rescaled 2PCFs. Notes that, results of BBN + BAO are the same in left and right panels. The grey dotted lines indicate cosmological parameters used for mock construction. The contours show the 68 (1 σ) and 95 per cent (2 σ) confidence intervals. The red star indicates a parameter set at the 1 σ edge of the BAO constraints, but excluded by the LP measurements at more than 2 σ level.

	true	BAO	LP
H_0 (km s $^{-1}$ Mpc $^{-1}$)	67.77	$71.4^{+4.4}_{-7.8}$	$75.3^{+4.4}_{-8.7}$
Ω_m	0.307115	$0.376^{+0.091}_{-0.131}$	$0.459^{+0.146}_{-0.141}$

Table 5. The best-fitting cosmological parameters and 1 σ confidence intervals of LP and BAO measured from mean 2PCFs of Patchy mocks. The cosmological parameters used for mock construction are shown in 'true' column.

the observational data. The marginalized posterior distributions of α and y_{LP} are illustrated in Figure 9.

We find that the posterior distributions obtained from pre- and post-reconstruction data are concentrated at clearly different values, especially for posterior distributions of y_{LP} , which did not occur in posterior distributions fitted from mean 2PCFs of mocks (see Figure 3). This may be due to the higher level of noise in the SDSS

data compared to the mock data. Figure 10 shows the distribution of Δy and $\Delta y/\sigma_y$. We can find that the measurements of the SDSS data are all within the shaded areas and the $\Delta y/\sigma_y$ of the SDSS data are less than 1, indicating that the measurements from the SDSS data are not outliers compare to the corresponding mock data.

The measured y_{LP} and α are presented in Table 6. We find that the statistical errors of the observed data are smaller than those of the mocks. It could be due to the nonlinear damping of the BAO peak, which has the potential to magnify the uncertainty of BAO position. For all samples, the errors of the LP measurements are slightly higher than those of the corresponding BAO measurements. The statistical error would be reduced by reconstruction, but the reduction in bin $z \in [0.5, 0.75]$ is not as significant as in the corresponding mocks, only 5–11 per cent, resulting in a reduction of σ_{comb} is 8–11 per cent. Measuring LP from rescaled 2PCFs increases the statistical error by 4–11 per cent, and increases the σ_{comb} by 3–15 per cent. It should be noted that additional scale-dependent observational systematic

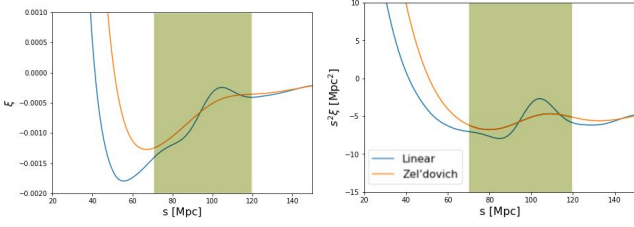


Figure 6. The 2PCFs generated with extraordinary cosmology which illustrated with red star in left panel of Figure 5. The blue lines are linear 2PCFs and the orange lines indicate the Zel'dovich approximated 2PCFs. The green shaded area refer to the range we searching for BAO peak and its associated left dip. The left panel shows plain 2PCFs (ξ) while the right panel shows rescaled 2PCFs ($s^2\xi$). the blue solid and orange solid line indicates linear and Zel'dovich-approximated 2PCFs, respectively. The green shadow area indicates our peak and dip search range defined as $[0.7r_d, 1.2r_d]$, here $r_d = 97.3$ Mpc.

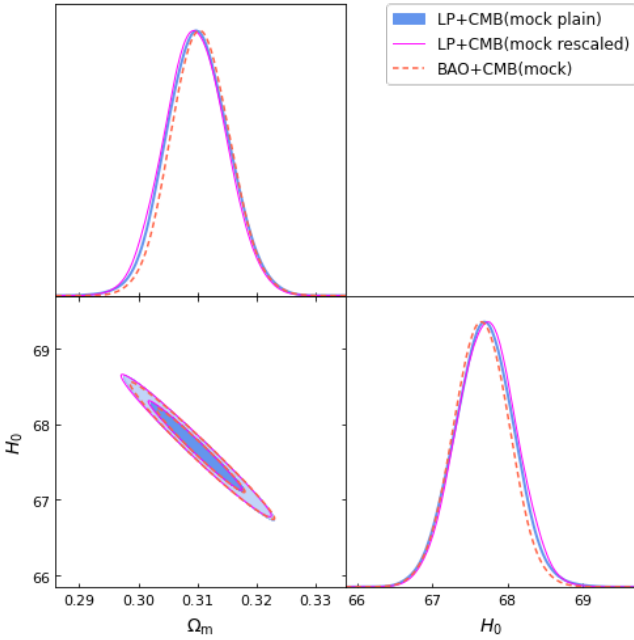


Figure 7. Constraints on H_0 and Ω_m based on the combination of BBN, CMB and LP (or BAO) measurements from reconstructed mocks. The LP results from the plain and rescaled 2PCFs are shown in blue and magenta, respectively. The red contour and lines show constraints with CMB + BAO. The blue contour and lines show constraints from CMB + LP (plain), where LP are measured from plain 2PCFs, the green contour and lines show constraints from CMB + LP (rescaled), where LP are measured from rescaled 2PCFs, while the red dashed contour and lines show that of CMB + BAO.

error biases the clustering on large scale significantly compare to the prediction by the mock data (see Ross et al. 2017). Although the BAO measurements are not sensitive to such observational errors, as the broad-band effects are accounted for by the nuisance parameters, they may make the LP measurements worse since y_{LP} is directly measured from the fitted polynomial. This indicates that the standard BAO measurements should be more reliable than the LP measurements. We will examine cosmological constraints to ensure the consistency of our results in the following section.

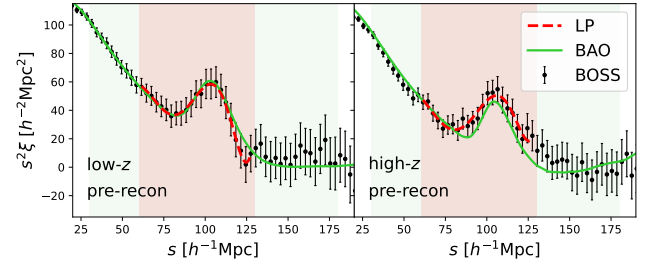


Figure 8. Same as Figure 2, but the measured 2PCFs with error bars and the best-fitting results of the SDSS data.

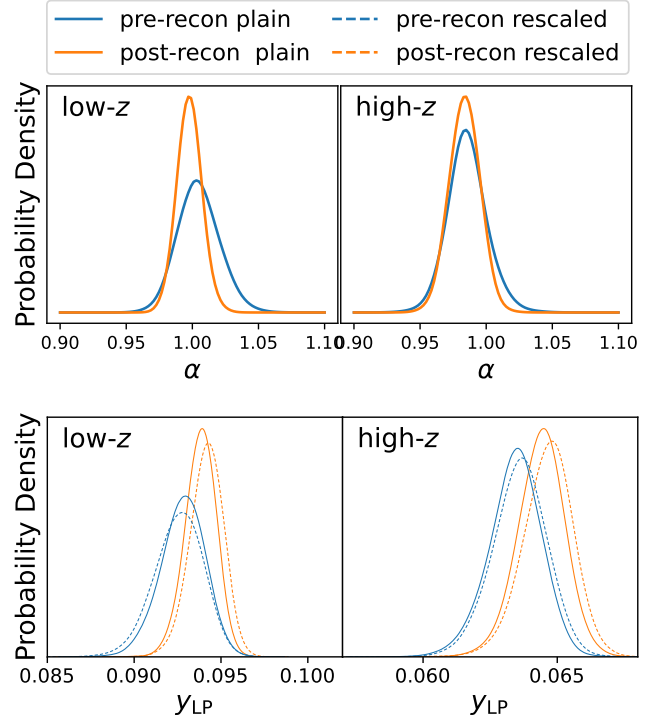


Figure 9. Same as Figure 3, but for marginalized posterior distributions of α and y_{LP} fitted from SDSS data.

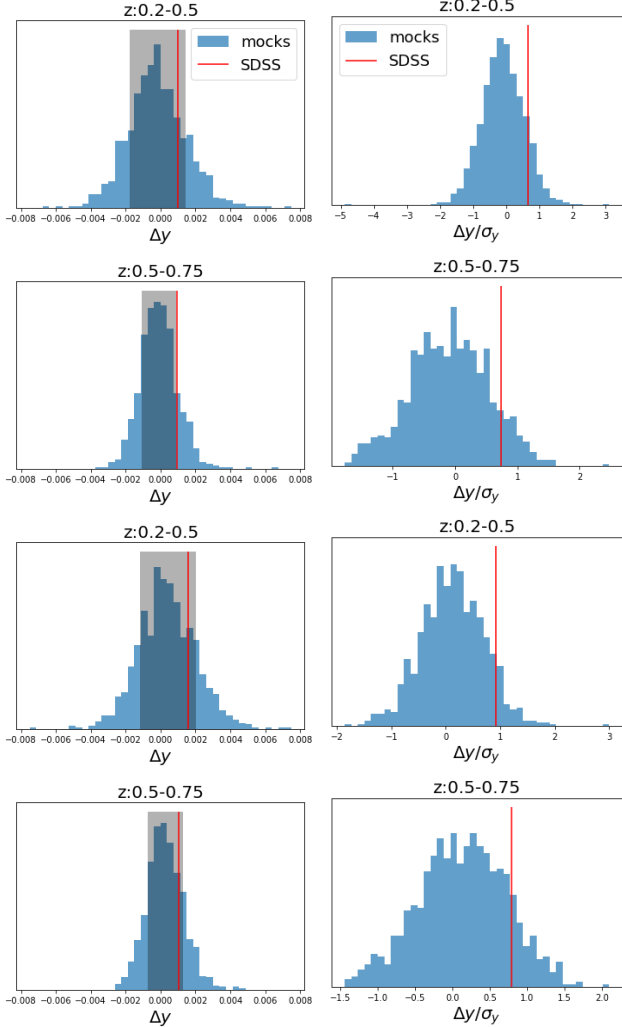
5.2 Cosmological parameter measurements

We present the constraints of the cosmological parameters in the standard flat- Λ CDM model by combining the BBN and Planck CMB data with our measurements in Figure 11 and Table 7.

When combined with BBN, the LP and BAO constraints are similar for Ω_m . However, there is a tension on the H_0 parameter. This can be explained by the fact that the LP is not be detectable with extreme Ω_m and H_0 values (see Section 4.5). The result with the LP show 3.3 per cent larger 1σ confidence interval on constraints of H_0 than that of BAO, while the 1σ constraint on Ω_m is 0.5 per cent better.

We conclude that the LP is useful for cosmological measurements when combined with additional datasets that provide reasonably tight constraints on the parameters, such that the BAO peak is prominent. Under this condition, the constraints from the LP are similar to those of the BAO. But the LP benefits from the fact that a cosmology-dependent template is not necessary. We also note that with the Laguerre reconstruction method introduced by Nikakhtar et al. (2021), the determination of the LP is more robust so that the requirement

SDSS DR12	measurement	best-fitting	Δ	σ	σ_{comb}	$\sigma_{\text{comb}}(\%)$	$\frac{\chi^2}{\text{d.o.f.}}$
post (low-z)	$100 \times y_{\text{LP}}(\xi)$	9.385	0.019	0.089	0.091	0.97%	0.94
	$100 \times y_{\text{LP}}(s^2\xi)$	9.421	0.044	0.096	0.105	1.12%	
	α	0.9977	0.0015	0.009	0.010	0.95%	
post (high-z)	$100 \times y_{\text{LP}}(\xi)$	6.443	0.013	0.086	0.087	1.35%	1.10
	$100 \times y_{\text{LP}}(s^2\xi)$	6.470	0.026	0.091	0.095	1.47%	
	α	0.9837	0.0036	0.012	0.013	1.30%	

Table 6. The measurements of y_{LP} and α for observed SDSS data.**Figure 10.** Differences in the measured y_{LP} (Δy_{LP}) and $\Delta y/\sigma_y$ between pre- and post-reconstruction. The blue histograms show measurements from individual mocks, the red vertical lines denote results from SDSS data and the grey shadows in left panels show the range between lower and upper 1σ confidence intervals which evaluated from the 16th, and 84th percentiles of the Δy of mocks.

on additional datasets may be released. We leave a dedicated study to the future work.

6 CONCLUSIONS

In this paper, we propose several novel schemes for measuring LP, such as using reconstructed data, rescaled 2PCFs ($s^2\xi$), and esti-

Data	H_0 (km s $^{-1}$ Mpc $^{-1}$)	Ω_m
BBN + BAO	$81.0^{+7.4}_{-9.6}$	$0.483^{+0.117}_{-0.112}$
BBN + LP (rescaled)	$77.9^{+4.8}_{-9.3}$	$0.454^{+0.116}_{-0.132}$
CMB	67.37 ± 0.54	0.3147 ± 0.0074
CMB + BAO	$67.87^{+0.35}_{-0.34}$	$0.3075^{+0.0046}_{-0.0046}$
CMB + LP (plain)	$68.00^{+0.36}_{-0.35}$	$0.3057^{+0.0045}_{-0.0046}$

Table 7. The best-fitting cosmological parameters and 1σ confidence intervals based on LP and BAO measured from SDSS observed data in combination with constraints from BBN and CMB.

imating statistical error with Bayesian sampling. We investigate the reliability, systematic bias, and statistical errors of these schemes with the help of approximate mock catalogues of SDSS DR12 LRG.

Following the method described in [Anselmi et al. \(2018b\)](#), we fit the monopole 2PCFs with a 5th-order polynomial, using an s bin width of $3 h^{-1}\text{Mpc}$ and a fitting range of $60\text{--}130 h^{-1}\text{Mpc}$. The LP measurements from individuals mocks show that about 23–40 per cent of plain pre-reconstruction 2PCFs are not measurable with S_{LP} due to the lack of a prominent BAO feature, making the LP measurements unreliable. This can be resolved by applying reconstruction or measuring S_{LP} from the rescaled 2PCFs, i.e., $s^2\xi$. For instance, with reconstruction, the S_{LP} -measurable rate increases by over ~ 95 per cent.

The y_{LP} predicted by the Zel’dovich approximation theory, denoted as $y_{\text{LP,zel}}$, is more consistent with y_{LP} measured from the mean 2PCFs of mocks for both pre- and post-reconstruction cases, compared to the theoretical value in linear theory. The systematic biases estimated using $y_{\text{LP,zel}}$ are less than 0.6 per cent for all measurement schemes. The statistical error measured with the Bayesian sampler is more stable than that of the error propagation method. Moreover, we find the median value of the posterior distribution to be a better indicator of the best-fitting result compared to the minimum- χ^2 value, by checking the consistency between measurements from individual mocks and the mean 2PCF of all mocks. Therefore, we use the median value and 1σ confidence interval obtained from the Bayesian sampler as our final LP measurements.

Taking into account both systematic and statistical errors, s_{LP} measured from reconstructed 2PCFs have slightly higher systematic bias compared to measurements from pre-reconstruction 2PCFs. Reconstruction can significantly reduce the statistical error by 20–30 per cent, resulting in a 25–32 per cent reduction in the combined error σ_{comb} . This indicates that BAO reconstruction increases the overall precision of LP measurements. Measuring LP from rescaled 2PCFs leads to a slight increase in both the systematic bias and statistical uncertainty of s_{LP} for the post-reconstruction case, resulting in a 4–8 per cent increase in the combined error.

We then compared the LP analysis with the standard BAO analysis using the mean 2PCFs of all mocks. The total relative error of y_{LP} is approximately 20–30 per cent higher than that of α . The cosmological

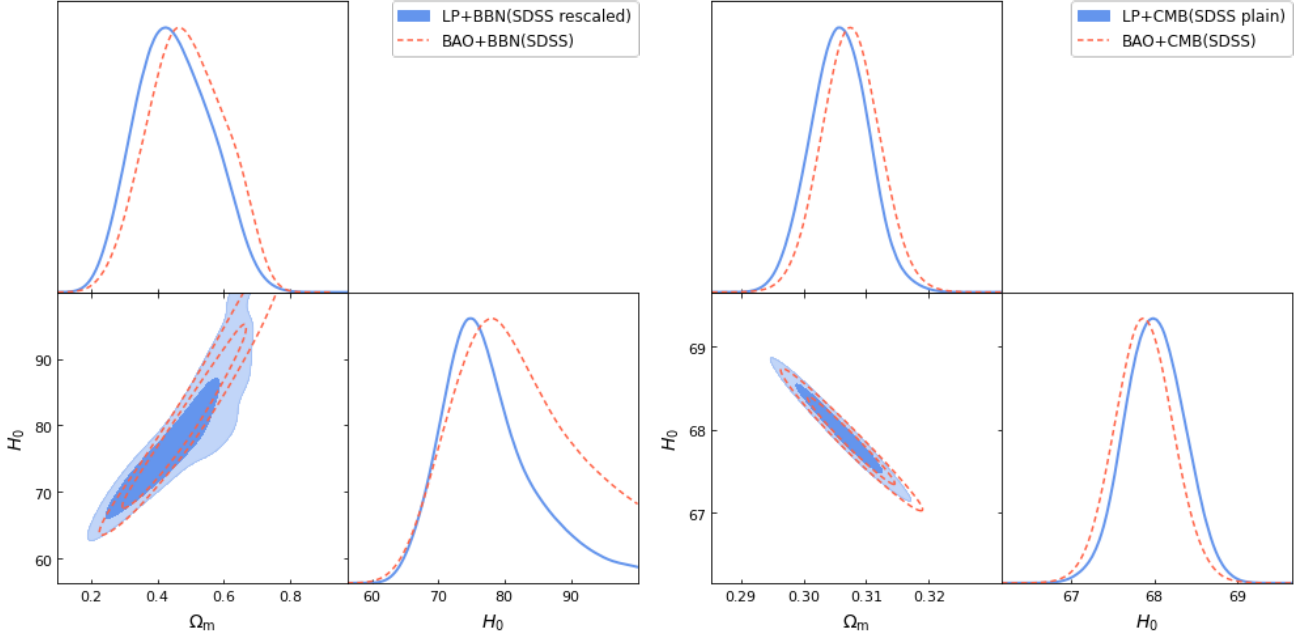


Figure 11. Constraints on H_0 and Ω_m based on the combinations of LP/BAO measurements from reconstructed SDSS data with BBN (left panel) and those with CMB (right panel).

results from combinations of BBN and LP measurements with the mean 2PCFs of mocks in the flat- Λ CDM cosmology indicate that, when LP is measured from plain 2PCFs, the posterior distribution of H_0 and Ω_m is restricted to lower values as the BAO peak is not always prominent when scanning the cosmological parameter space. This can be resolved by measuring the LP from rescaled 2PCFs. The constraints on Ω_m and H_0 of both BBN + LP (rescaled) and BBN + BAO are generally consistent. However, the BBN + LP (rescaled) measurements show a 0.57 and 0.62σ larger bias of the best-fitting value, as well as 21 and 3.6 per cent larger 1σ confidence interval for Ω_m and H_0 , respectively.

For SDSS data, the constraints from LP and BAO measurements are generally consistent. With the LP measurements based on quintic polynomial fitting method, the LP positions are not always detectable when cosmological parameter values are extreme, which results in unreliable constraints. This problem can be solved by including additional datasets such as CMB that constrain the parameter values in a relatively small volume so that the BAO peak is always prominent. In this case, the LP can produce results similar to those of traditional BAO measurements. When combined with CMB data (Planck Collaboration et al. 2020), we obtain $H_0 = 68.00^{+0.36}_{-0.35} \text{ km s}^{-1} \text{ Mpc}^{-1}$ and $\Omega_m = 0.3057^{+0.0045}_{-0.0046}$ with LP measurements from plain post-reconstruction 2PCFs, and $H_0 = 67.87^{+0.35}_{-0.34} \text{ km s}^{-1} \text{ Mpc}^{-1}$ and $\Omega_m = 0.3075^{+0.0046}_{-0.0046}$ with BAO measurements from the same data.

ACKNOWLEDGEMENTS

We acknowledge the support from the science research grants from the China Manned Space Project with No. CMS-CSST-2021-A01 and No. CMS-CSST-2021-B01. HYS acknowledges the support from NSFC of China under grant 11973070, Key Research Program of Frontier Sciences, CAS, Grant No. ZDBS-LY-7013 and Program of Shanghai Academic/Technology Research Leader.

DATA AVAILABILITY

All the code and data used to produce the analysis in this article are publicly available.

REFERENCES

- Abazajian K. N., et al., 2009, *ApJS*, **182**, 543
- Alam S., et al., 2017, *MNRAS*, **470**, 2617
- Anselmi S., Starkman G. D., Sheth R. K., 2016, *MNRAS*, **455**, 2474
- Anselmi S., Corasaniti P.-S., Starkman G. D., Sheth R. K., Zehavi I., 2018a, *Phys. Rev. D*, **98**, 023527
- Anselmi S., Starkman G. D., Corasaniti P.-S., Sheth R. K., Zehavi I., 2018b, *Phys. Rev. Lett.*, **121**, 021302
- Anselmi S., Starkman G. D., Renzi A., 2022, arXiv e-prints, p. arXiv:2205.09098
- Bassett B., Hlozek R., 2010, in Ruiz-Lapuente P., ed., , Dark Energy: Observational and Theoretical Approaches. p. 246
- Bautista J. E., et al., 2021, *MNRAS*, **500**, 736
- Carter P., Beutler F., Percival W. J., DeRose J., Wechsler R. H., Zhao C., 2020, *MNRAS*, **494**, 2076
- Cooke R. J., Pettini M., Steidel C. C., 2018, *ApJ*, **855**, 102
- Crocce M., Scoccimarro R., 2008, *Phys. Rev. D*, **77**, 023533
- DESI Collaboration et al., 2016, arXiv e-prints, p. arXiv:1611.00036
- Dawson K. S., et al., 2013, *AJ*, **145**, 10
- Eisenstein D. J., Hu W., Tegmark M., 1998, *ApJ*, **504**, L57
- Eisenstein D. J., et al., 2005, *ApJ*, **633**, 560
- Eisenstein D. J., et al., 2011, *AJ*, **142**, 72
- Foreman-Mackey D., Hogg D. W., Lang D., Goodman J., 2013, *PASP*, **125**, 306
- Gunn J. E., et al., 2006, *AJ*, **131**, 2332
- Kitaura F. S., Hess S., 2013, *MNRAS*, **435**, L78
- Kitaura F. S., Yepes G., Prada F., 2014, *MNRAS*, **439**, L21
- Kitaura F.-S., et al., 2016, *MNRAS*, **456**, 4156
- Landy S. D., Szalay A. S., 1993, *ApJ*, **412**, 64
- Laureijs R., et al., 2011, arXiv e-prints, p. arXiv:1110.3193
- Nikakhtar F., Sheth R. K., Zehavi I., 2021, *Phys. Rev. D*, **104**, 043530

- O'Dwyer M., Anselmi S., Starkman G. D., Corasaniti P.-S., Sheth R. K., Zehavi I., 2020, *Phys. Rev. D*, **101**, 083517
- Padmanabhan N., Xu X., Eisenstein D. J., Scalzo R., Cuesta A. J., Mehta K. T., Kazin E., 2012, *MNRAS*, **427**, 2132
- Planck Collaboration et al., 2020, *A&A*, **641**, A6
- Reid B., et al., 2016, *MNRAS*, **455**, 1553
- Ross A. J., et al., 2017, *MNRAS*, **464**, 1168
- Sánchez A. G., et al., 2012, *MNRAS*, **425**, 415
- Smee S. A., et al., 2013, *AJ*, **146**, 32
- Smith R. E., Scoccimarro R., Sheth R. K., 2008, *Phys. Rev. D*, **77**, 043525
- Xu X., Padmanabhan N., Eisenstein D. J., Mehta K. T., Cuesta A. J., 2012, *MNRAS*, **427**, 2146
- Zhao C., 2023, *arXiv e-prints*, p. arXiv:2301.12557
- Zhao C., et al., 2022, *MNRAS*, **511**, 5492

APPENDIX A: THE INFLUENCE OF FIDUCIAL COSMOLOGY

We investigate the influence of fiducial cosmology, which is used to convert the measured angles and redshifts into comoving coordinates, on the LP measurement with mocks. We measure y_{LP} from the 2PCFs of pre-reconstruction data with different fiducial $\Omega_m = \{0.12, 0.25, 0.31, 0.64, 0.85\}$. Ω_m is the key parameter used to convert the measured angular position and redshift into distance. The 2PCFs are calculated in the range of $s \in (0, 198) h^{-1} \text{ Mpc}$ with bin size of $3 h^{-1} \text{ Mpc}$. The y_{LP} are measured directly from 2PCFs rescaled by D_V . We show the mean $\xi(y)$ of mocks in Figure A1. It shows that $\xi(y)$ with different fiducial cosmologies are very similar at BAO scale.

Then we run polynomial fits for these $\xi(y)$ with the fitting range of $[60r_d/r_{d,\text{true}}, 130r_d/r_{d,\text{true}}] h^{-1} \text{ Mpc}$, here r_d is the comoving sound horizon at the drag epoch calculated with corresponding fiducial cosmology. Note that covariance matrices are rescaled by the number of mocks to ensure the statistical errors are negligible. The y_{LP} are estimated from searching $y_{\text{LP,peak}}$ and $y_{\text{LP,dip}}$ in the range $[75r_d/r_{d,\text{true}}, 115r_d/r_{d,\text{true}}] h^{-1} \text{ Mpc}$ with the method discussed in Section 3.2.

We show the systematic bias estimated from the linear theory predicted $y_{\text{LP,lin}}$ and Zel'dovich approximation predicted $y_{\text{LP,zel}}$ in Table A1. It shows that y_{LP} is closer to $y_{\text{LP,zel}}$ for all cases. If the fiducial Ω_m happens to be the true value, the systematic errors are less than 0.2 per cent. Even with most extreme value of Ω_m , the systematic biases are less than 0.6 per cent. For the measurements from rescaled 2PCFs ($s^2\xi(y)$), the systematic errors are below 0.1 per cent if the value of Ω_m is not far from the true one. This indicates that the influence on y_{LP} from fiducial cosmology are very small, that can be negligible comparing to statistical error with the samples used in this work.

This paper has been typeset from a \LaTeX file prepared by the author.

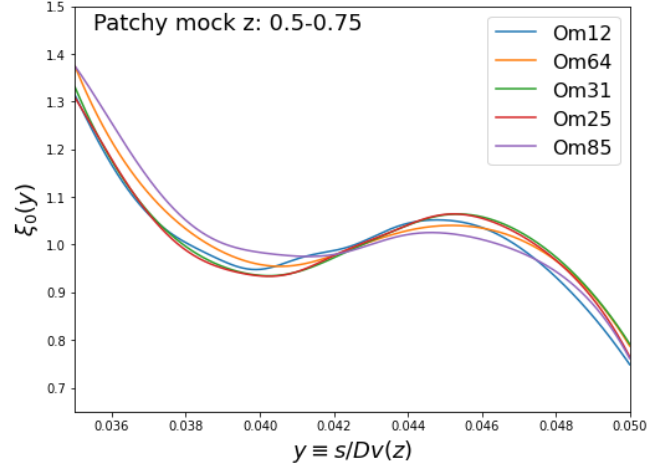


Figure A1. The mean 2PCFs of Patchy mocks computed with different fiducial cosmologies.

Ω_m	$y_{LP}(\xi)$	$y_{LP}(s^2\xi)$	$\Delta y_{lin}(\xi)$	$\Delta y_{lin}(s^2\xi)$	$\Delta y_{zel}(\xi)$	$\Delta y_{zel}(s^2\xi)$
0.12	0.06281	0.06269	1.734%	2.176%	0.387%	0.555%
0.25	0.06311	0.06299	1.257%	1.712%	0.096%	0.084%
0.31	0.06320	0.06308	1.123%	1.570%	0.231%	0.061%
0.64	0.06330	0.06317	0.961%	1.427%	0.396%	0.206%
0.85	0.06341	0.06319	0.799%	1.389%	0.560%	0.244%

Table A1. The impact of Ω_m (fiducial cosmology) in the measured y_{LP} and its bias Δy . Δy are defined as $y - y_{theory}$, for Δy_{lin} and the expected values of y_{LP} are estimated from linear theory predicted 2PCFs, while Δy_{zel} they are predicted by Zel'dovich-approximated 2PCFs. The columns with (ξ) show measured values directly from 2PCFs, while columns with $(s^2\xi)$ show values from rescaled 2PCFs. Each y_{LP} is measured from the best-fitting mean 2PCF of the 2048 pre-reconstruction Patchy mocks.